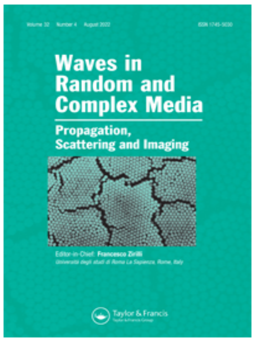

Waves in Random and Complex Media

ISSN: (Print) (Online) Journal homepage: https://www.tandfonline.com/loi/twrm20

Transport of drugs using complex peristaltic waves in a biological system

Nouman Ijaz, Ahmed Zeeshan, Arshad Riaz & Mohammed Sh. Alhodaly

WAVES IN RANDOM AND COMPLEX MEDIA
https://doi.org/10.1080/17455030.2022.2111031

Transport of drugs using complex peristaltic waves in a biological system

Nouman Ijaz [a], Ahmed Zeeshan[b], Arshad Riaz [c] and Mohammed Sh. Alhodaly[d]

[a]Department of Mathematics and Statistics, Punjab Group of Colleges, Jhelum, Pakistan; [b]Department of Mathematics and Statistics, FBAS, International Islamic University, Islamabad, Pakistan; [c]Department of Mathematics, Division of Science and Technology, University of Education, Lahore, Pakistan; [d]Department of Mathematics, Faculty of Science, Nonlinear Analysis and Applied Mathematics (NAAM)-Research Group, King Abdulaziz University, Jeddah, Saudi Arabia

ABSTRACT

Targeted drugging in view of diseases, such as cancer, diabetes, and cardiovascular diseases. etc., has become vitally important. This theoretical analysis intricates the transport of drugs using Peristaltic micro-pumps and is controlled by a magnetic field in pharmacological engineering. The current article analyzed small drug particles embedded in a non-Newtonian fluid in a partially permeable space enclosed between flexible walls. To control the transport process magnetic force lines are applied at a right angle to the flow direction. The transportation of liquid along with drug particles due to the peristaltic movement of walls of a channel is modeled, simulated, and analyzed. Considering the flow assumptions and conditions, a second-order system of partial differential equations (PDEs) is devised to describe the flow. The numerical simulation using pdepe is established and graphically displayed for the effects of different parameters.

ARTICLE HISTORY
Received 25 February 2022
Accepted 20 July 2022

KEYWORDS
Durg transport; biphase nanofluid; magnetohydrodynamics; pharmacological delivery systems

1. Introduction

Targeted drug delivery, also called smart drugging is a phenomenon, which enhances the number of drugs in affected parts of the body as compared to the rest of the body. As in the case these drugs can be used to stop cancer signals that help to grow cancer cells. Usually, nano medication is used in this pharmacological transport mechanism. This medication is more effective as it targets the affected tissues only and reduces the number of medicines needed and their side effects on healthy tissues. The only downside seems to be the high cost of these systems. Recently Liu, et al. [1] discussed in their novel study on this drug system and its potential. A review of different drug delivery systems was done by Manish and Vimukta [2]. A few recent studies are [3–5] and herein. Lai et al. [6] investigated the alginate-based complex fibers with the Janus morphology for the controlled release of co-delivered drugs.

CONTACT Nouman Ijaz noumanijaz666@gmail.com

Peristaltic transport is a procedure to transport fluid due to persistent contraction and relaxation, creating a propagating wave along the tube/duct containing fluids. These phenomena exist naturally in the human body for the transport of food. Inspired by this many devices, such as, heart-lung machines, PDMS peristaltic micropump, etc., are developed. It is employed in applications, such as sanitary transport, blood pumps, pharma transport systems, etc. The pioneer work done by Latham [7] leads to numerous inquiries [8–12] allocated in the domain of peristaltic flow.

Multiphase fluids tend to appear in most of the flows that saw in industry or natural flows. One of the applications is liquid particle suspension that appears in flood or flow sand or clay in water. The term 'multiphase fluids' stands for systems with different substances or different phases of matter that may coexist. The flow of a single-phase fluid is well understood and developed over the years. Many results are published both theoretically and experimentally. However, this implication does not effectively hold for bi/multiphase flows, due to interference and interactive forces of all the phases. The factors, such as shape, size, concentration, physical and chemical properties, etc., of phases involved effects and complicate the flow of multiphase fluids. Hence, the available theories of such biphase flows are only restricted to the general level. To control these multiphase flows, extensive learning of such mechanisms is needed. Suspensions of solid dust particles could be observed in multiple flow situations, with examples in biological systems, such as blood, household goods, such as paints, and industrial processing such as waste slurry. Many of these flows are of great importance in energy and environmental engineering fields. Many theoretical and experimental studies [13–23] in recent times show the importance of the current field of research.

Non-Newtonian fluids are proved to be relatively much applicable in the various present-day and physiological fields. Blood flow, polymer rheology, stoneware, and ketchup are specific illustrations of non-Newtonian fluids. One of the large classes of fluids described by the Power-law model can also work to exhibit a shear thickening feature. In many cases, the Ree–Eyring fluid proves to be more useful than power-law type models. The interesting thing is to note that the Ree–Eyring fluid approaches to viscous fluid properties both for high and lesser shear ratios and its basic condition can also be procured by dynamic speculation of liquid as opposed to the testing association. These different features add to the applicability of the Ree-Erying fluid model. Khan et al. [24] report the flow topographies of the Ree-Eyring fluid among two disks that are rotating subject to the constant transverse magnetic field. They also address entropy generation effects accompanied by radiation. Hayat et al. [25] also studied entropy generation in the presence of chemically reactive material. Hayat et al [26] explored the Ree-Eyring fluid rheology in biologically inspired peristaltic transport with homogenous-heterogeneous chemical reactions. Ijaz et al. [27] extended the work in a duct and added heat transfer later on. Safarpouret al. [28] studied Wave propagation characteristics of a cylindrically laminated composite nanoshell in a thermal environment based on the nonlocal strain gradient theory.

Ijaz et al. [29] committed the peristaltic stream of Eyring-Powell Nanofluid in a deviated channel. Robins-type (convective) conditions are utilized within the site of blended convection and magnetic field. The fundamental conditions of the Eyring-Powell Nanofluid are displayed in the wave frame of reference. Khan et al. [30] evaluated the flow of the Ree-Eyring fluid over a stretching parabolic surface. Tanver and malik [31] worked with the slip effect in a curved geometry. While an infinitely spinning disk was assumed by Al-Mdallal et al. [32]; they also assumed Cu nanoparticles suspended in fluid. Temperature-dependent viscosity effects were unriddled by Yousif and Ali [33]. Bhatti et al. [34] investigated the wall properties in the flow of the Ree-Eyring fluid in a channel with a progressive peristaltic wave. They combined the effects of Lorentz force and slip boundary conditions to unriddle this problem. Zeeshan et al. [35] communicated about endoscopic measures along with homogeneous-heterogeneous aspects in the magnetized peristaltic analysis of the Ree-Eyring fluid. Scientific exhibiting and examination have been performed utilizing tube-formed headings. Inspections are made on the basis that the catching bolus increases for greater estimation of the porous parameter. A. Muhammadi [36] examined the influence of the viscoelastic foundation on the dynamic behavior of the double-walled cylindrical inhomogeneous microshell using MCST and and GDQM. Hina et al. [37] worked on the Powell-Eyring fluid in a curve geometry with a transverse magnetic field.

Considering the applicability and focus of the literature in such a flow problem authors are motivated to establish the current analysis. In this article, the peristaltically inspired flows of Ree-Eyring non-compressible, steady fluid with non-conducting drug particles are considered. The subsequent problem for the liquid and particle stages is handled using the Eigenfunction expansion strategy. The outcomes are examined with the assistance of diagrams.

2. Quantitative formulation

In this work, the sinusoidal progressive wave phenomenon of an incompressible and uniformly distributed particulate suspension in the Ree-Eyring steady and irrotational fluid running with a velocity c is presented. The material is assumed to be a good conductor of electricity. An externally applied consent field due to the permanent magnetic is undertaken perpendicular to the X-axis. The flow problem is demonstrated in the cartesian coordinate system with the X-axis reflected parraellal with the flow and the others are admitted to normal it as shown in Figure 1. Mathematically,

$$\tilde{Z} = \tilde{H}\left(\ddot{X}, \ddot{t}\right) = \pm a \pm b_1 \cos\left[\frac{2\pi}{\lambda}\left(\ddot{X} - c\ddot{t}\right)\right] \pm b_2 \cos\left[\frac{4\pi}{\lambda}\left(\ddot{X} - c\ddot{t}\right)\right], \tag{1}$$

Here, ‘a’ is the distance from the origin to a stationary wall, and ‘b’ is the amplitude of the wave, ‘c’ is the wave speed, and ‘λ’ is the wavelength.

The mathematical model of the ReeEyring fluid model is [38]

$$T_{ij} = \mu_s \frac{\partial \widetilde{V}_j}{\partial \tilde{x}_i} + \frac{1}{\overline{\overline{B^*}}} ArcSinh\left(\frac{1}{\overline{\overline{C}}}\frac{\partial \widetilde{v}_j}{\partial \tilde{x}_i}\right). \tag{2}$$

$Sinh^{-1}\Theta \approx \Theta$ when $|\Theta| \leq 1$,Reduced Equation 2 becomes

$$T_{ij} \approx \left(\mu_s + \frac{1}{\overline{\overline{B^*}}}\left(\frac{1}{\overline{\overline{C}}}\right)\right)\frac{\partial \widetilde{V}_j}{\partial \tilde{x}_i} \tag{3}$$

Now we develop a new frame moving with a similar speed to that of a wave relative to the static frame, which is defined as

$$\ddot{X} \to \widetilde{x} + c * \ddot{t}, \widetilde{Z} \to \widetilde{z}, \widetilde{Y} \to \widetilde{y}, \widetilde{P} \to \widetilde{p}, \widetilde{U}_{f,p} \to \widetilde{u}_{f,p} + c. \tag{4}$$

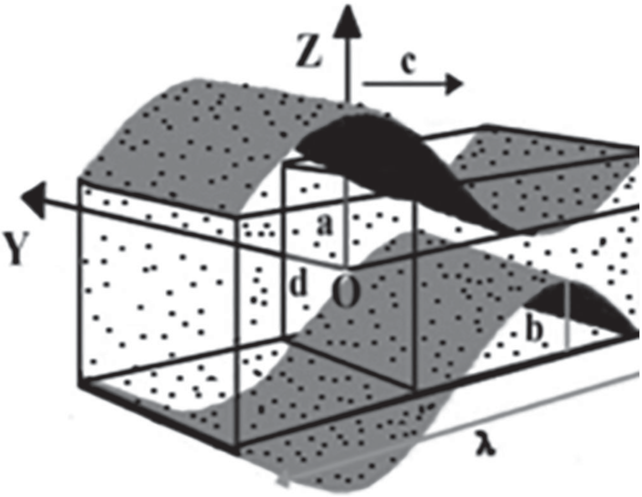

Figure 1. Geometrical structure.

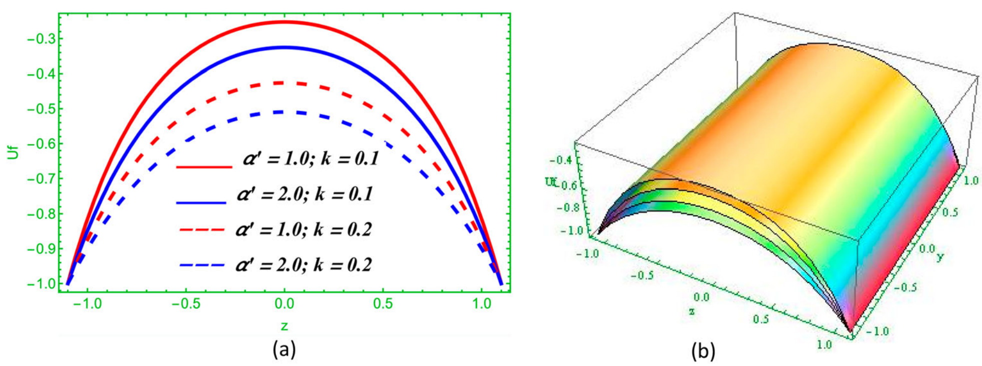

Figure 2. u_f curves for increasing value of $\alpha' andk$. When $C = 0.1$, $\beta = 0.1$, $M = 0.2$. (a) For two-dimensional, (b) For three-dimensional.

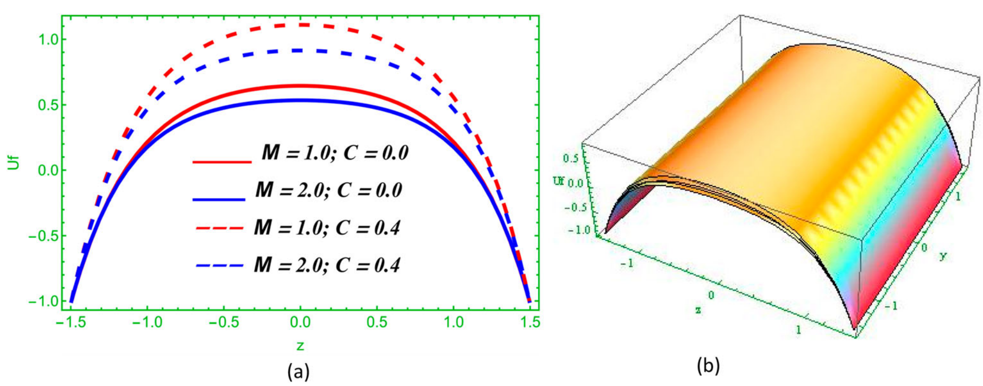

Figure 3. u_f curves for increasing value of $CandM$. When $\alpha' = 0.1$, $\beta = 0.1$, $k = 0.2$. (a) For two-dimensional, (b) For three-dimensional.

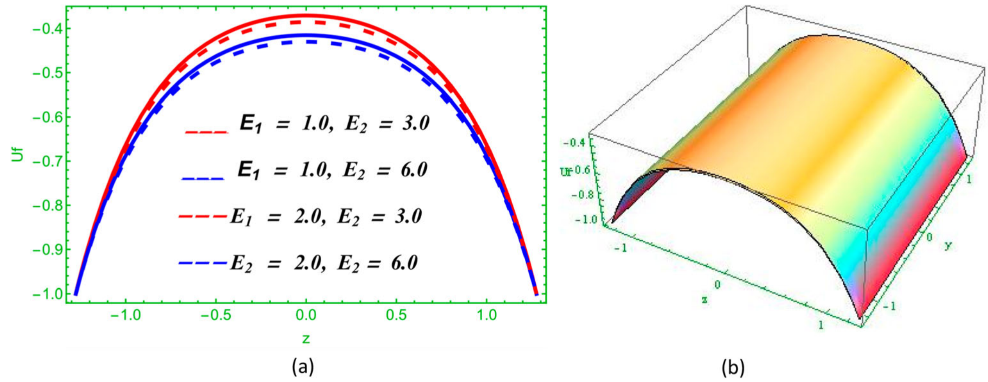

Figure 4. u_f curves for increasing value of $E_1 and E_2$. When $C = 0.1$, $\beta = 0.1$, $M = 0.2$. (a) For two-dimensional, (b) For three-dimensional.

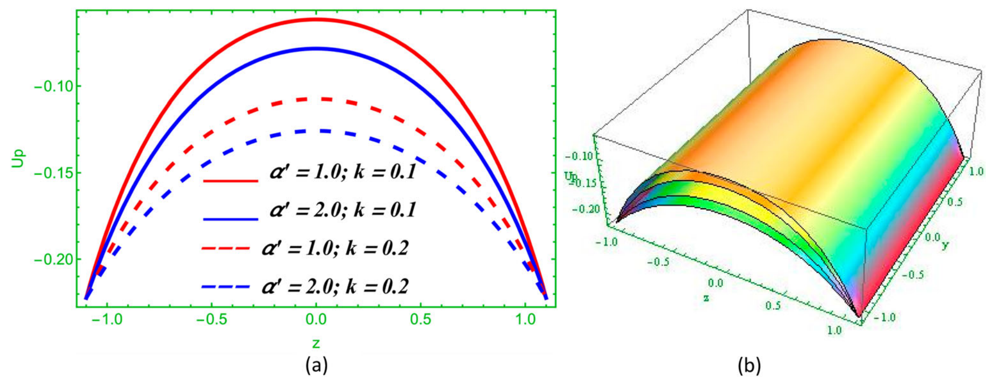

Figure 5. u_p curves for increasing value of $\alpha' and k$. When $C = 0.1$, $\beta = 0.1$, $M = 0.2$. (a) For two-dimensional, (b) For three-dimensional.

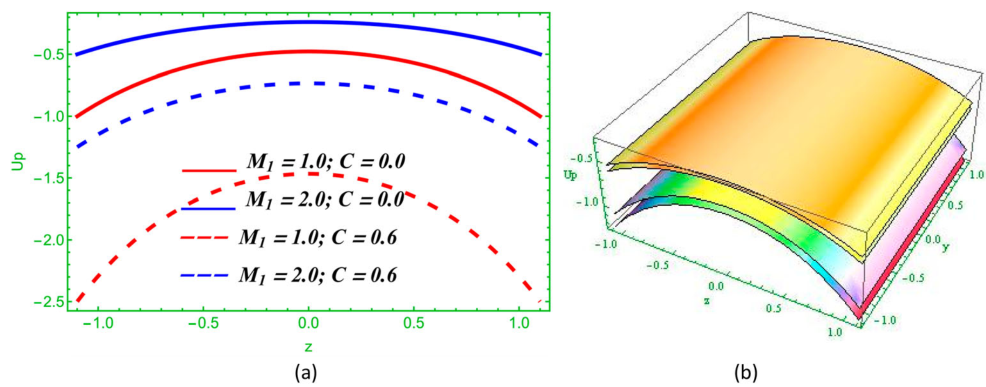

Figure 6. u_p curves for increasing value of $C and M$. When $\alpha' = 0.1$, $\beta = 0.1$, $k = 0.2$. (a) For two-dimensional, (b) For three-dimensional.

Outlining the non-dimensional parameters:

$$x = \lambda^{-1}\tilde{x}, y = d^{-1}\tilde{y}, z = a^{-1}\tilde{z}, u_{f,p} = c^{-1}\tilde{u}_{f,p}, w_{f,p} = (c\delta)^{-1}\tilde{w}_{f,p}, t = \lambda^{-1}\tilde{ct},$$

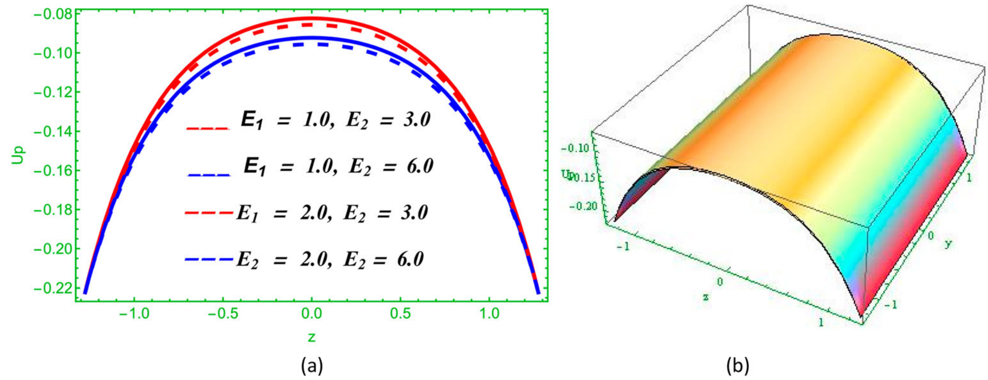

Figure 7. u_p curves for increasing value of $E_1 and E_2$. When $C = 0.1$, $\beta = 0.1$, $M = 0.2$. (a) For two-dimensional, (b) For three-dimensional.

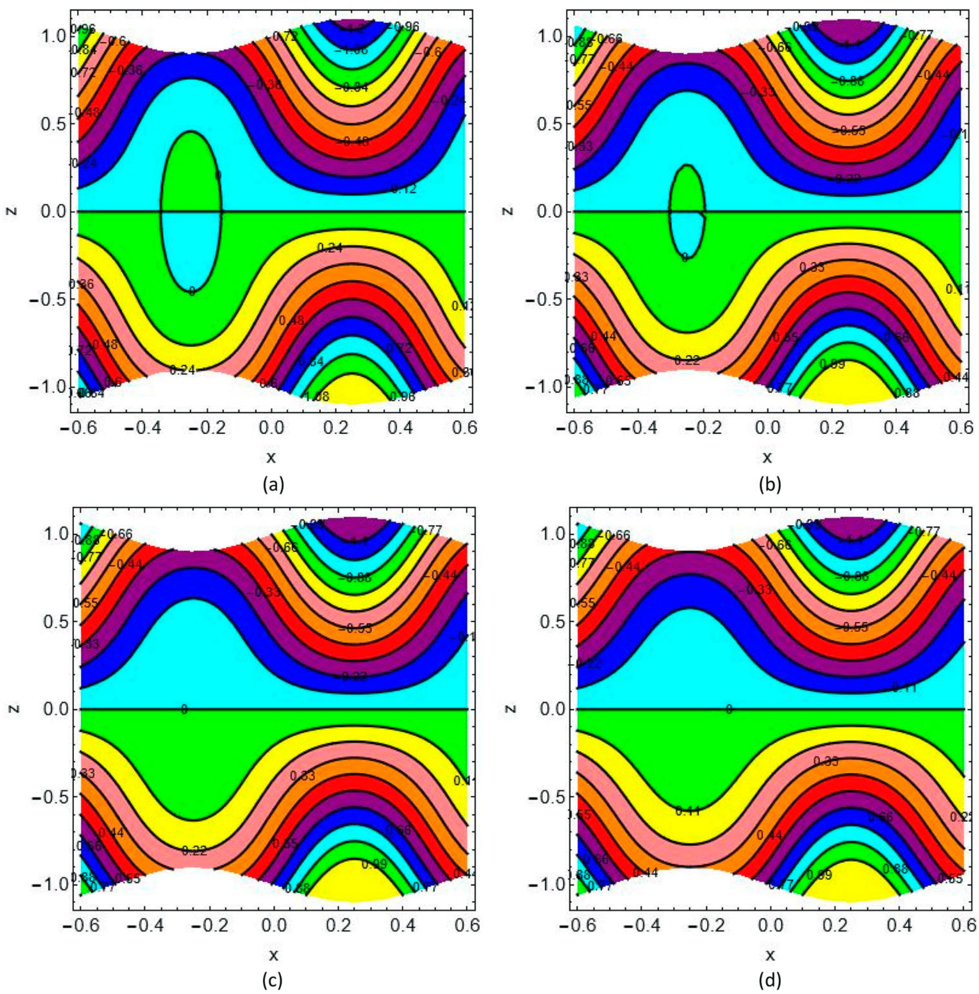

Figure 8. Streamlines of u_f for a few values of $\alpha' = 0.1, 0.2, 0.3, 0.4$.

$$\widetilde{h} = a^{-1}H, \varphi = ba^{-1}, p = \frac{a^2\widetilde{p}}{uc\lambda}, \delta = \frac{a}{\lambda}, \beta = \frac{a}{d}, Re = \frac{\rho\delta ca}{\mu}, M_1 = \frac{a^2 S'}{\mu_s}(1-C)^{-1},$$
$$M^2 = \frac{\sigma(a\beta_0)^2}{\mu}, \alpha' = \frac{1}{C\mu_s B'}, \bar{k} = \frac{k}{a^2}, \mathrm{T}_{xx} = \frac{a}{\mu c}\widetilde{\mathrm{T}}_{\widetilde{x}\widetilde{x}}, \mathrm{T}_{xz} = \frac{a}{\mu c}\widetilde{\mathrm{T}}_{\widetilde{x}\widetilde{z}}, \mathrm{T}_{xy} = \frac{d}{\mu c}\widetilde{\mathrm{T}}_{\widetilde{x}\widetilde{y}},$$
$$\mathrm{T}_{yz} = \frac{d}{\mu c}\widetilde{\mathrm{T}}_{\widetilde{y}\widetilde{z}}, \mathrm{T}_{yy} = \frac{\lambda}{\mu c}\widetilde{\mathrm{T}}_{\widetilde{y}\widetilde{y}}, \mathrm{T}_{zz} = \frac{\lambda}{\mu c}\widetilde{\mathrm{T}}_{\widetilde{z}\widetilde{z}}. \tag{5}$$

Here, x,y, and z are special coordinate axis, u and w are velocity components, t is the time, H is the wave shape, ϕ is the phase lag, p is the pressure, δ is the wave number, λ is the wavelength, β is the aspect ratio, R_e is the Reynolds number, M_1 is the particles interaction parameter, S' is the drag force, C is the volume fraction, M is the magnetic parameter, and k is the porosity.

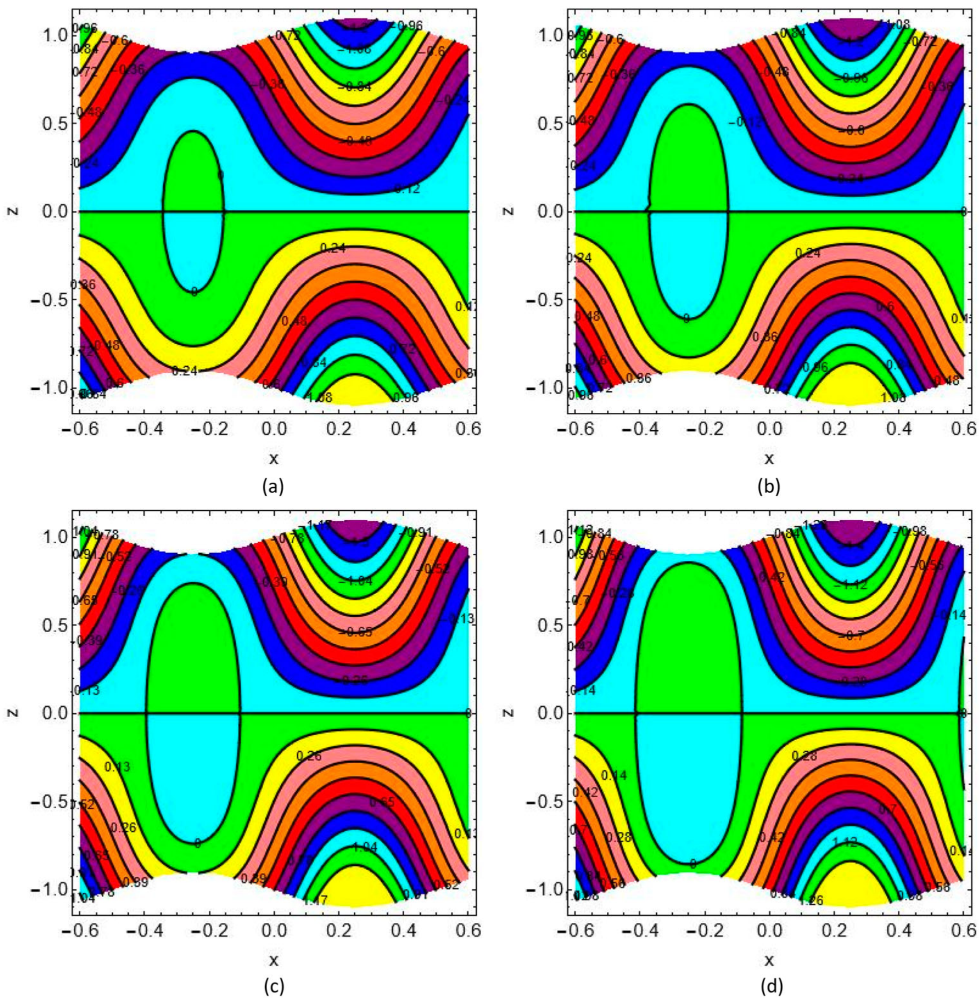

Figure 9. Streamlines of u_f for a few values of $C = 0.1, 0.2, 0.3, 0.4$.

Using Equations (2–5) into the governing equations defined in [39,40] and after dropping the tilde, the resulting equations are

$$\frac{\partial u_f}{\partial x} + \frac{\partial w_f}{\partial z} = 0, \tag{6}$$

$$Re\left(u_f \frac{\partial u_f}{\partial x} + w_f \frac{\partial u_f}{\partial w}\right) = -\frac{\partial p}{\partial x} + \delta \frac{\partial \mathrm{T}_{xx}}{\partial x} + \beta^2 \frac{\partial \mathrm{T}_{xy}}{\partial y} + \frac{\partial \mathrm{T}_{xz}}{\partial z} - \frac{M^2(u_f+1)}{(1-C)} - \frac{1}{k}\frac{(u_f+1)}{(1-C)} - M_1(u_p - u_f), \tag{7}$$

$$Re\delta\left(u_f \frac{\partial u_f}{\partial x} + w_f \frac{\partial u_f}{\partial w}\right) = -\frac{\partial p}{\partial z} + \delta^2\left(\frac{\partial \mathrm{T}_{zx}}{\partial x} + \frac{\beta^2}{\delta}\frac{\partial \mathrm{T}_{zy}}{\partial y} + \frac{\partial \mathrm{T}_{zz}}{\partial z} - \frac{CM_1}{\delta}(w_p - w_f)\right), \tag{8}$$

$$\frac{\partial u_p}{\partial x} + \frac{\partial w_p}{\partial z} = 0, \tag{9}$$

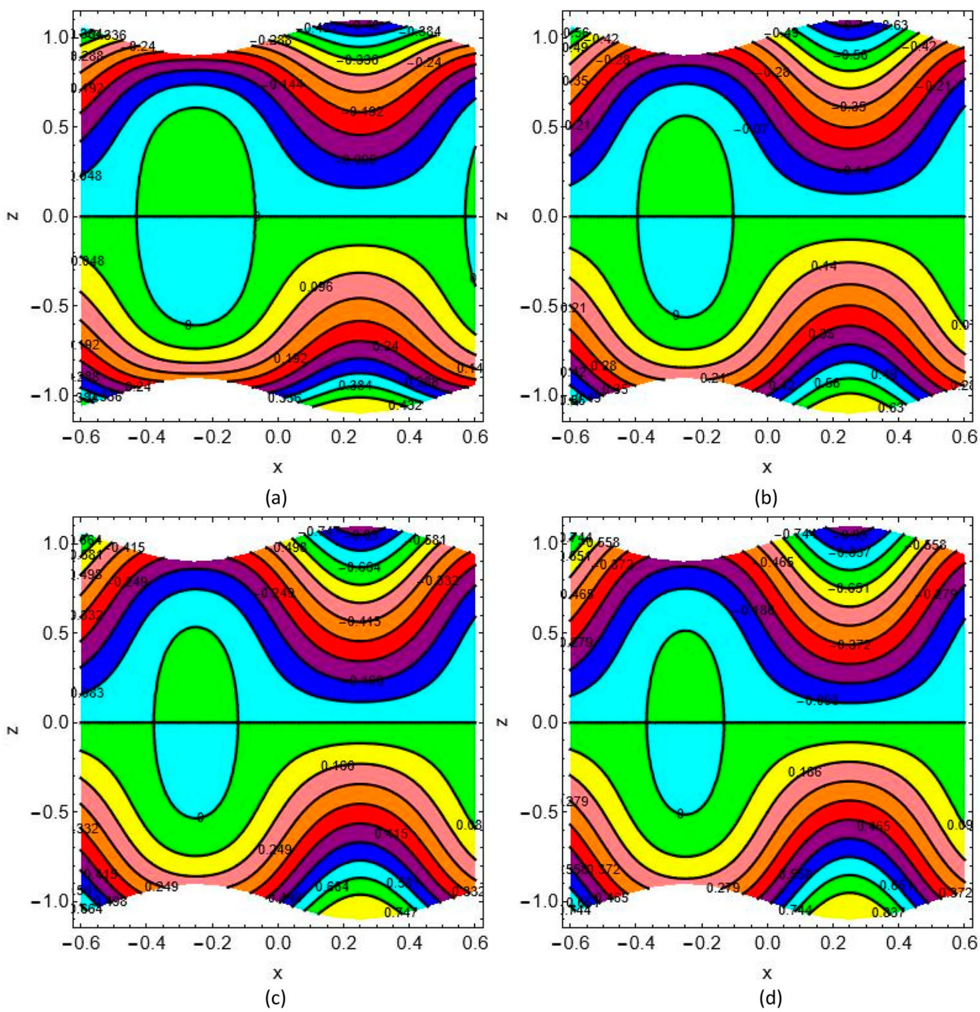

Figure 10. Streamlines of u_f for a few values of $k = 0.1, 0.2, 0.3, 0.4$.

$$Re\left(u_p\frac{\partial u_p}{\partial x}+w_p\frac{\partial u_p}{\partial w}\right)=-\frac{\partial p}{\partial z}+(1-C)M_1(u_f-u_p), \tag{10}$$

$$Re\delta\left(u_p\frac{\partial w_p}{\partial x}+w_p\frac{\partial w_p}{\partial w}\right)=-\frac{\partial p}{\partial z}+\delta M_1(1-C)(w_f-w_p). \tag{11}$$

The corresponding relations for the drag and viscosity of the mixture were demonstrated as

$$\left.\begin{aligned} S' &= \frac{9\mu_0}{2a^2}\lambda(C),\\ \lambda(C) &= (2-3C)^{-2}(4+3(8C-3C^2)^{0.5}+3C),\\ \mu_s &= \frac{\mu_0}{1-\chi C'},\\ \chi &= 7\times10^{-2}e^{[2.49C+1107e^{-1.69C}T^{-1}]} \end{aligned}\right\} \tag{12}$$

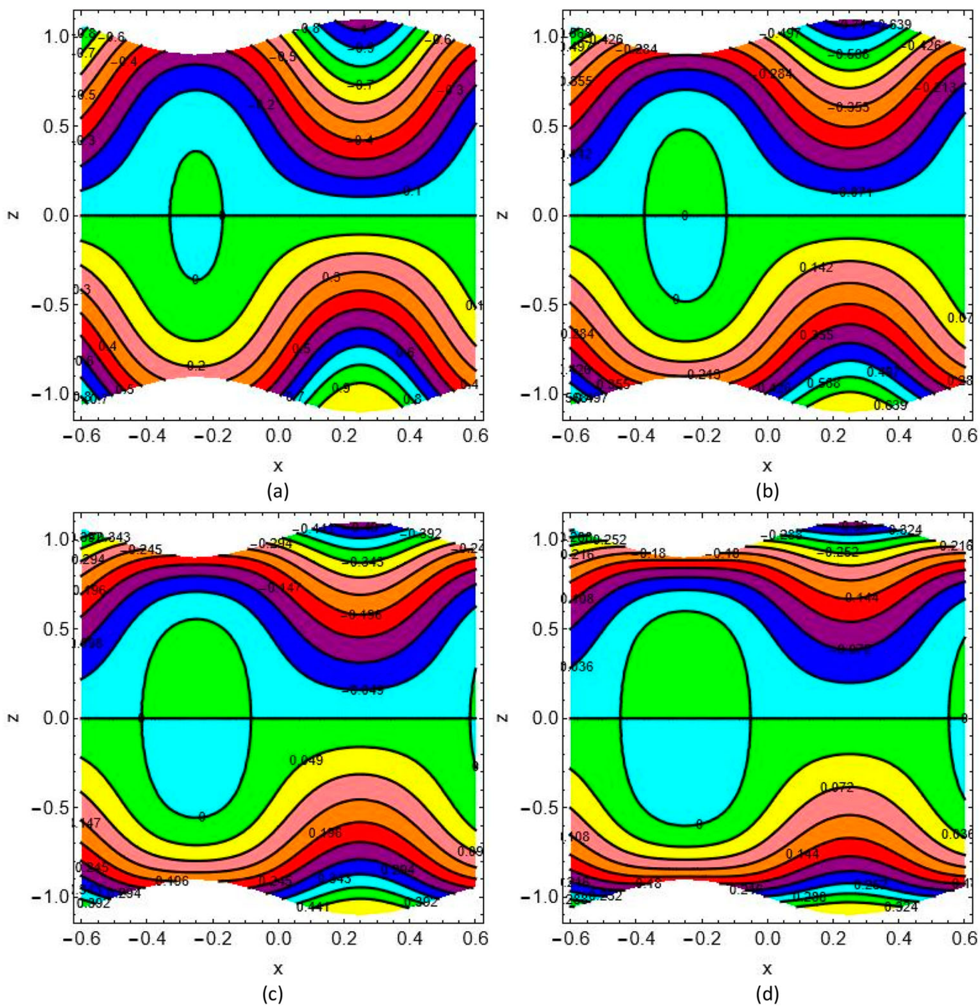

Figure 11. Streamlines of u_f for a few values of $M = 1.0, 2.0, 3.0, 4.0$.

Assuming creeping flow and long-wavelength readings in Equations (6–12), the concluding equations for the two phases can be written as

$$\beta^2(1+\alpha')\frac{\partial^2 u_f}{\partial y^2}+(1+\alpha')\frac{\partial^2 u_f}{\partial z^2}-\frac{1}{k}-M^2u_f=\frac{dp}{dx}+\frac{1}{k}u_f+CM_1(u_p-u_f)+M^2 \tag{13}$$

$$(1-C)u_p=-\frac{1}{M_1}\frac{dp}{dx}+(1-C)u_f \tag{14}$$

The boundaries of the channel satisfy the following physical assumptions

$$u_f(x,y,z)=\left\{\begin{matrix}-1, & \text{at } y=\pm 1,\\ -1\ at\ z=\pm h(x)=\pm(1+\varphi_1\cos 2\pi)+(1+\varphi_2\cos 4\pi)\end{matrix}\right\}. \tag{15}$$

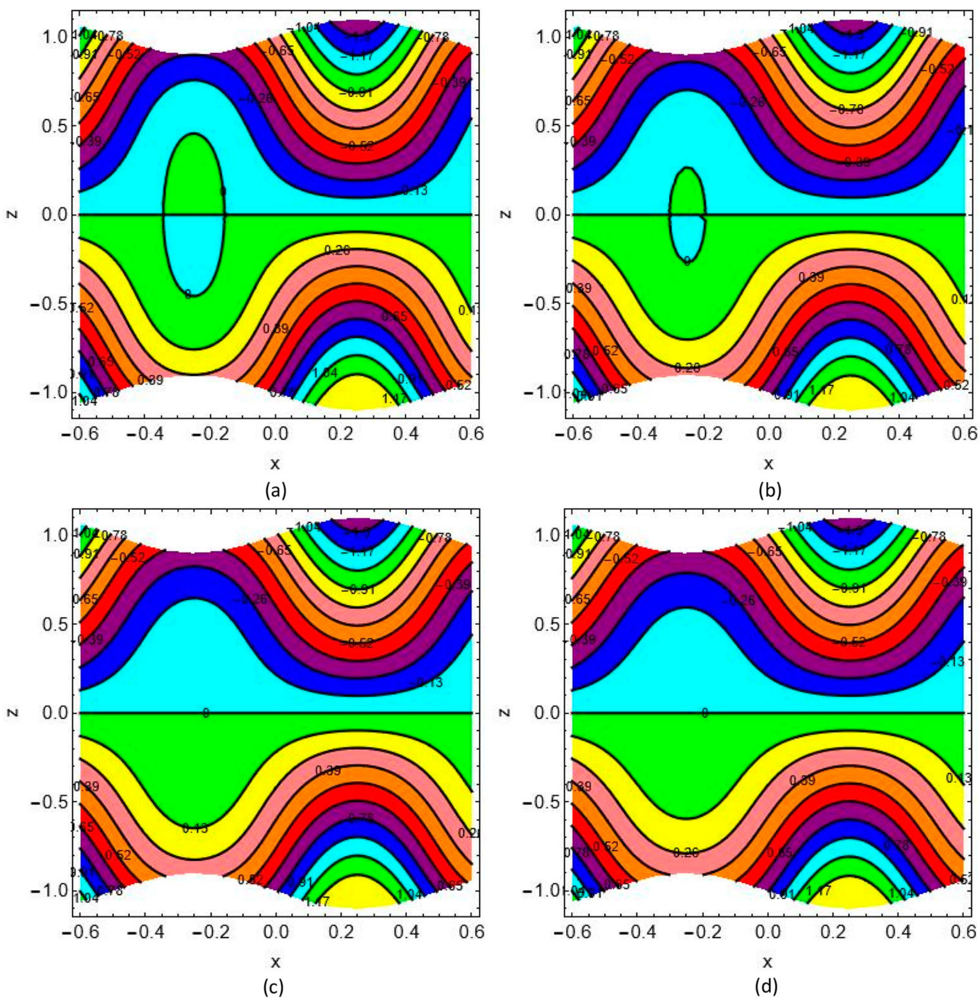

Figure 12. Streamlines of u_p for a few values of $\alpha' = 0.1, 0.2, 0.3, 0.4$.

3. Results and discussion

In this section, a detailed description of graphic trends and resultant numerical evaluation using 'pdepe' for the flow problem modeled using particle-fluid two-phase formulation for drug particle in the Ree-Eyring non-Newtonian fluid model with changeable flow controlling parameters, such as the Hartmann number M, drug particle volume concentration C, the Ree-Eyring fluid rheological parameter α', and Drag force due to particles M_1. Velocity and streamlines in the dynamics of the designed particle-fluid model are evaluated and graphically represented. Figures 2–7 show 2D and 3D graphs for the velocity of fluid and particle separately for the varying values of controlling parameters. Whereas, Figures 8–15 depict variation in bolus formation and streamlines due to defined parameters.

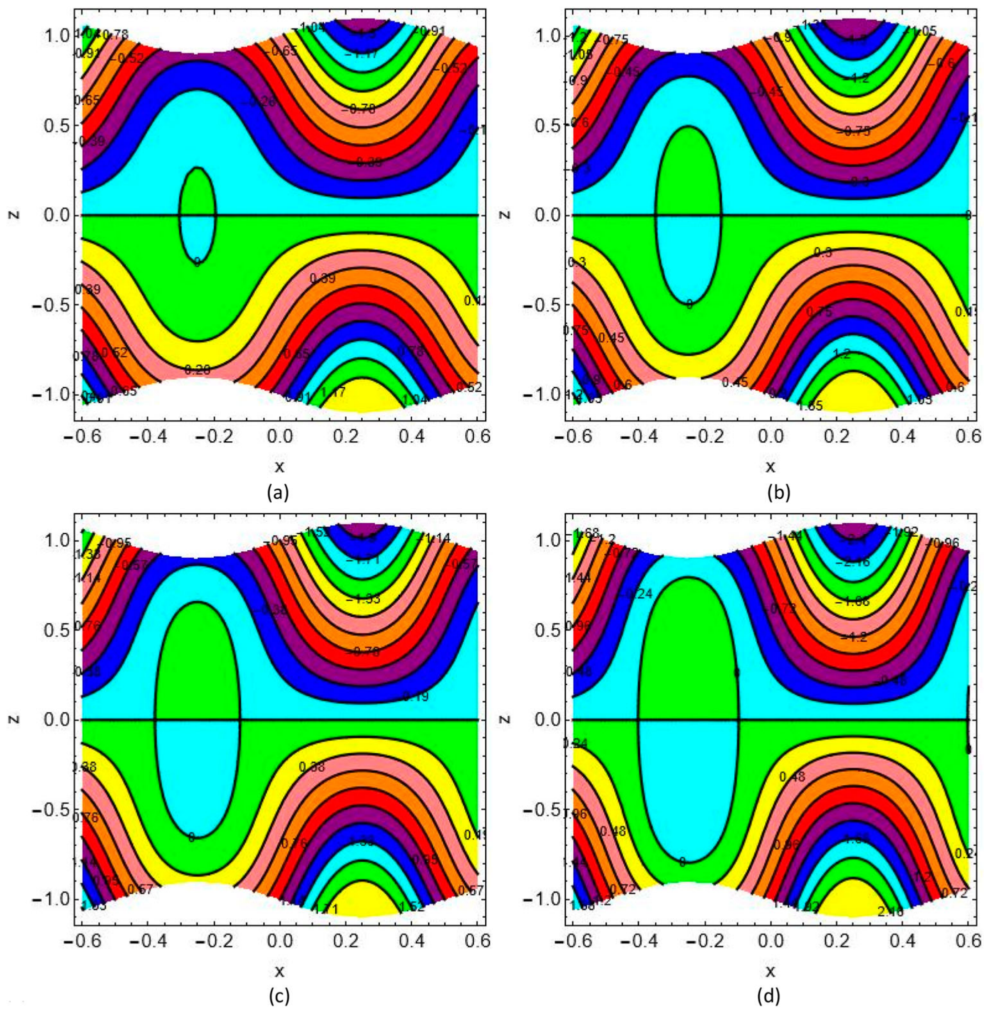

Figure 13. Streamlines of u_p for a few values of $C = 0.1, 0.2, 0.3, 0.4$.

3.1. Velocity profiles

Figures 2–4 show the variation of fluid velocity, while 5–7 show particle velocity. Figure 2, shows that speed diminishes with an increment in the Ree-Eyring rheological parameter α', also fluid velocity tends to reduce with the permebilty parameter k of porous space. This parameter emerges due to the Darcian drag term $-\frac{1}{k}(u_f + 1)$ that emerges in Equation 7, since the flow is in porous spaces, also the flow creeps ignoring higher-order terms. The drag incrporated with higher permeability values allows the fluid to pass easily. Velocity profiles for different values of the Hartmann number M and drug particle concentration can be seen in Figure 3. When the value of the magnetic field parameter M increases, fluid velocity decreases. It is the opposite for particle concentration, due to the rise of a resistive force called Lorentz force. This force drags the fluid by generating magnetic lines of forces when applied perpendicularlyhence slows down the flow. Its effect is evident at the peak of the flow speed. Here $[-M^2(u_f + 1)]$ emerges in the fluid phase momentum Equation

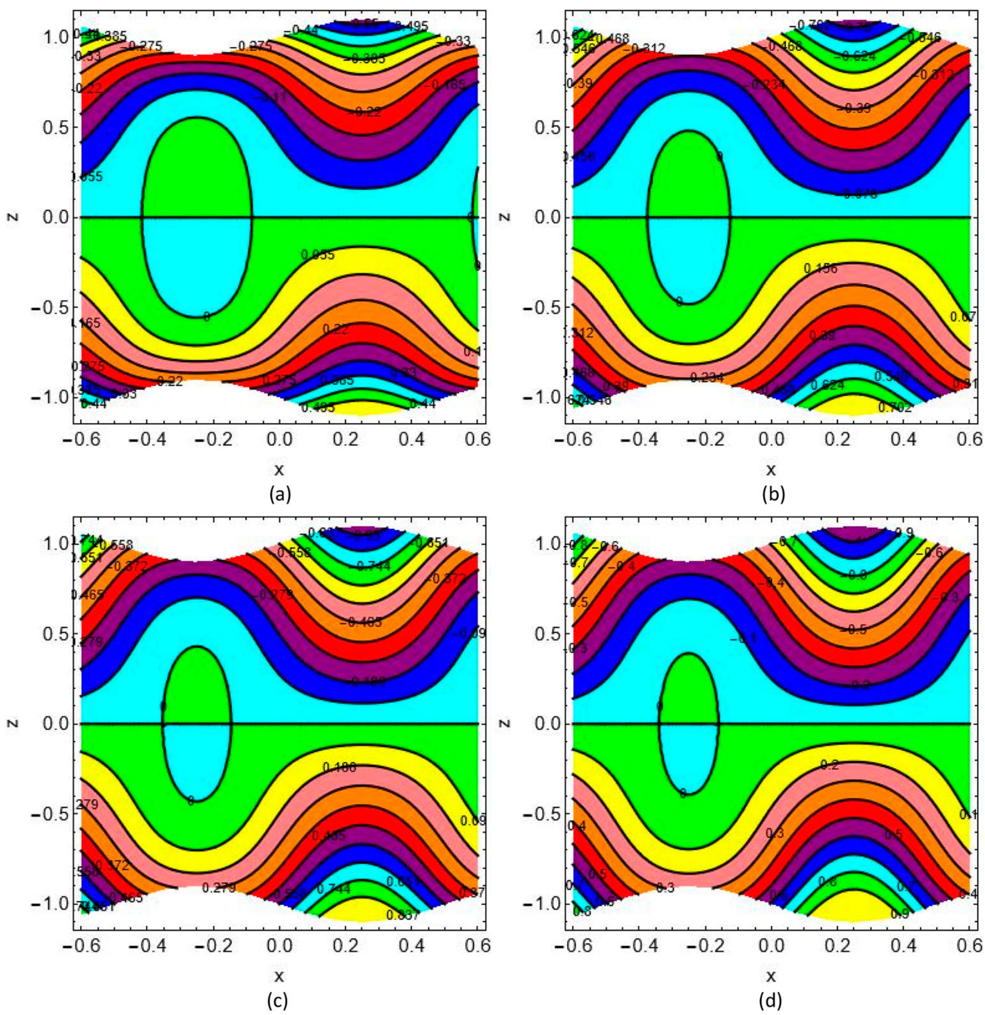

Figure 14. Streamlines of u_p for a few values of $k = 0.1, 0.2, 0.3, 0.4$.

(7). Whereas, an increase in the electric field accelerates the velocity of the fluid particles. Figure 4 explicitly exhibits a raise in velocity for the elasticity parameter E_1 and wall mass factor E_2.

Figure 5 shows that the Ree-Eyring fluid parameter α' gives slower velocity nearer to the lower wall. Furthermore, it is revealed that the traveling of solid segments is in line with that of fluid flow. Meanwhile, if solid particles with negligibly small mass are considered, the particle's velocity intensity reduces. Figure 6 displays that by enlarging the particle parameter C, the speed of fluid also slows down. Likewise, as the drag number M_1 drives up, particles travel slower. Figure 7 offers a look at a particulate velocity in axial direction under the variation of wall measurements E_1 and E_2.

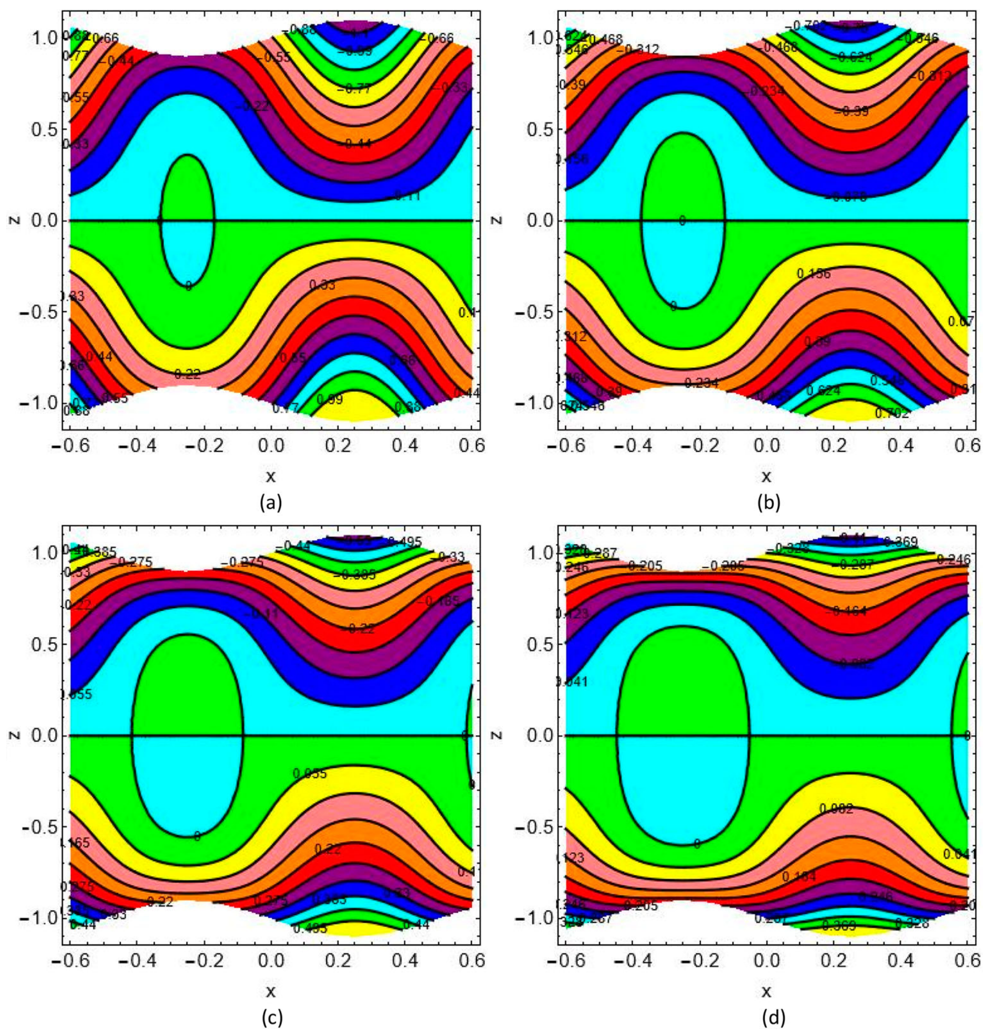

Figure 15. Streamlines of u_p for a few values of $M = 1.0, 2.0, 3.0, 4.0$.

3.2. Streamlines

The level curves of stream function adjacent to moving wave boundaries assumed the character of walls. However, streamlines are closed contours in the middle region called a bolus. The development of the fluid bolus by circumscribed streamlines is known as the trapping phenomenon. The bolus tends to move along the direction of the peristaltic wave. Figures 8 and 12 display the impact of α' on the trapping of both fluid and particles. The size of the bolus diminishes for larger values of α'. It is shown in Figure 9 https://www.sciencedirect.com/science/article/pii/S0169260719311435 – fig0020 that bolus size is significantly stimulated by *C*. The circulation bolus is boosted with a rise in C. Similar results are observed for particle concentration in Figure 13. However, Figures 10 and 14 demonstrate the bolus size was reduced for rising values of *k*. The bolus size shows a rise in size if M is increased (Figure 11), Also the size increases for a particulate flow (Figure 15).

4. Conclusion

In the current article, analytical investigations examining the effects of magnetism on the transport of the Ree-Erying fluid with embedding drug particles due to periodic sinusoidal wave on the wall are modeled. A transport of this solid-liquid mixture through a porous rectangular duct with compliant walls is assumed. The quantitative problem that governs fluid and solid phases is articulated in the light of some physical constraints, such as lubrication assumption and arterial dimensions, supposed for the enclosure. The problem is particularly suited to the pharmacological transport of drugs using non-Newtonian fluids. The exact solution strategy was adopted to find the results of all differential equations and put them in a final closed form. The technique described for this treatment is the Eigenfunction expansion method. The following cumulative results have been observed.

- It can be declared that velocity factors for fluid as well as particles are being reduced because of magnetic force, part size, and wall compliance.
- It has been noticed that the Ree-Erying parameter and porosity measures enhance the velocity profiles which can be admissible both in two-and three-dimensional frames.
- It is also noticeable here that fluid parameter and porosity enlarge, and the size and number of the trapped boluses decreases, but inverse observation is collected in the case of volume fraction of particles and the Hartman number.
- It is also admitted that the same kind of information is obtained for the bolus phenomenon of the particulate phase for the parameters of attentiveness.

Disclosure statement

No potential conflict of interest was reported by the author(s).

ORCID

Nouman Ijaz http://orcid.org/0000-0002-8729-6670
Arshad Riaz http://orcid.org/0000-0003-0717-6677

References

[1] Liu D, Yang F, Xiong F, et al. The smart drug delivery system and its clinical potential. Theranostics. 2016;6(9):1306–1323.
[2] Manish G, Vimukta S. Targeted drug delivery system: a review. Res J Chem Sci. 2011;1(2):135–138.
[3] Saraf S. Applications of novel drug delivery system for herbal formulations. Fitoterapia. 2010;81(7):680–689.
[4] Gupta BP, Thakur N, Jain NP, et al. Osmotically controlled drug delivery system with associated drugs. J Pharm Pharm Sci. 2010;13(4):571–588.
[5] Kingsley JD, Dou H, Morehead J, et al. Nanotechnology: a focus on nanoparticles as a drug delivery system. J Neuroimmune Pharmacol. 2006;1(3):340–350.
[6] Lai W, Huang E, Lui K. Alginate-based complex fibers with the Janus morphology for controlled release of co-delivered drugs. Asian J Pharm Sci. 2021;16(1):77–85.
[7] Latham, T.W. MS Thesis, MIT, USA; 1966.
[8] Fung YC, Yih CS. ASME J. Appl. Mech. 1968;35:669–675.
[9] Barton C, Raynor S. Peristaltic flow in tubes. Bull. Math. Biophys. 1968;30:663–680.
[10] Shapiro AH, Jafferin MY, Weinberg SL. Peristaltic pumping with long wavelengths at low Reynolds number. J. Fluid Mech. 1969;37:799–825.
[11] Tripathi D, Bég OA. A study on peristaltic flow of nanofluids: application in drug delivery systems. Int J Heat Mass Transfer. 2014;70:61–70.
[12] Riaz A, Zeeshan A, Bhatti MM, et al. Peristaltic propulsion of Jeffrey nano-liquid and heat transfer through a symmetrical duct with moving walls in a porous medium. Physica A. 2020;545:123788.
[13] Kumar R, Kumar A, Goel V. Effect of rounded corners on heat transfer and fluid flow through triangular duct. J Heat Transfer. 2018;140:12.
[14] Zeeshan A, Ijaz N, Bhatti MM, et al. Mathematical study of peristaltic propulsion of solid–liquid multiphase flow with a biorheological fluid as the base fluid in a duct. Chin J Phys. 2017;55(4):1596–1604.
[15] Mekheimer KS. Peristaltic transport of a particle–fluid suspension through a uniform and non-uniform annulus. Appl Bionics Biomech. 2008;5(2):47–57.
[16] Sinnott MD, Cleary PW, Harrison SM. Peristaltic transport of a particulate suspension in the small intestine. Appl Math Model. 2017;44:143–159.
[17] Chu KW, Yu AB. Numerical simulation of complex particle–fluid flows. Powder Technol. 2008;179(3):104–114.
[18] Lai W, Wong W. Property-tuneable microgels fabricated by using flow-focusing microfluidic geometry for bioactive agent delivery. Pharmaceutics. 2021;13(6):787.
[19] Shariati A, Habibi M, Tounsi A, et al. Application of exact continuum size-dependent theory for stability and frequency analysis of a curved cantilevered microtubule by considering viscoelastic properties. Eng Comput. 2021;37:3629–3648.
[20] Al-Furjan MSH, Habibi M, Safarpour H. Vibration control of a smart shell reinforced by graphene nanoplatelets. Int J Appl Mech. 2020;12(06):2050066.
[21] Lai W, Huang E, Lui K. Alginate-based complex fibers with the janus morphology for controlled release of co-delivered drugs. Asian J Pharm Sci. 2021;16(1):77–85. doi:10.1016/j.ajps.2020.05.003.
[22] Moayedi H, Ebrahimi F, Habibi M, et al. Application of nonlocal strain–stress gradient theory and GDQEM for thermo-vibration responses of a laminated composite nanoshell. Eng Comput. 2021;37:3359–3374.
[23] SafarPour H, Hosseini M, Ghadiri M. Influence of three-parameter viscoelastic medium on vibration behavior of a cylindrical nonhomogeneous microshell in thermal environment: An exact solution. J Therm Stresses. 2017;40(11):1353–1367.
[24] Khan MI, Khan SA, Hayat T, et al. An. Int J Numer Methods Heat Fluid Flow. 2019;30(4):1839–1865.
[25] Hayat T, Khan SA, Khan MI, et al. Theoretical investigation of Ree–Eyring nanofluid flow with entropy optimization and Arrhenius activation energy between two rotating disks. Comput Methods Programs Biomed. 2019;177:57–68.
[26] Hayat T, Akram J, Alsaedi A, et al. Endoscopy and homogeneous-heterogeneous reactions in MHD radiative peristaltic activity of Ree-Eyring fluid. Results Phys. 2018;8:481–488.

[27] Ijaz N, Zeeshan A, Bhatti MM. Peristaltic propulsion of particulate non-Newtonian Ree-Eyring fluid in a duct through constant magnetic field. Alexandria Eng J. 2018;57(2):1055–1060.

[28] Safarpour H, Ghanizadeh SA, Habibi M. Wave propagation characteristics of a cylindrical laminated composite nanoshell in thermal environment based on the nonlocal strain gradient theory. Eur Phys J Plus. 2018;133:532.

[29] Ijaz N, Bhatti MM, Zeeshan A. Heat transfer analysis in magnetohydrodynamic flow of solid particles in non-Newtonian Ree-Eyring fluid due to peristaltic wave in a channel. Therm Sci. 2019;23(2 Part B):1017–1026.

[30] Khan MI, Kadry S, Chu YM, et al. Exploration of Lorentz force on a paraboloid stretched surface in flow of Ree-Eyring nanomaterial. J Mater Res Technol. 2020;9(5):10265–10275.

[31] Tanveer A, Malik MY. Slip and porosity effects on peristalsis of MHD Ree-Eyring nanofluid in curved geometry. Ain Shams Eng J. 2021;12(1):955–968.

[32] Al-Mdallal QM, Renuka A, Muthtamilselvan M, et al. Ree-Eyring fluid flow of Cu-water nanofluid between infinite spinning disks with an effect of thermal radiation. Ain Shams Eng J. 2021;12(3):2947–2956.

[33] Yousif R, Ali HA. Temperature-Dependent viscosity effect on the peristaltic transport of (MHD) blood flow Ree-Eyring fluid through porous medium in an inclined asymmetric channel. Al-Qadisiyah J Pure Sci. 2020;25(3):16–34.

[34] Bhatti MM, Abbas MA, Rashidi MM. Combine effects of Magnetohydrodynamics (MHD) and partial slip on peristaltic blood flow of Ree–Eyring fluid with wall properties. Eng Sci Technol. an Int J. 2016;19(3):1497–1502.

[35] Zeeshan A, Bhatti MM, Muhammad T, et al. Magnetized peristaltic particle–fluid propulsion with Hall and ion slip effects through a permeable channel. Physica A. 2020;550:123999.

[36] Mohammadi A, Lashini H, Habibi M, et al. An. J Solid Mech. 2019;11(2):440–453.

[37] Hina S, Mustafa M, Hayat T, et al. Peristaltic transport of Powell–Eyring fluid in a curved channel with heat/mass transfer and wall properties. Int J Heat Mass Transfer. 2016;101:156–165.

[38] Riaz A, Ellahi R, Sait S. M. Role of hybrid nanoparticles in thermal performance of peristaltic flow of Eyring–Powell fluid model. J Therm Anal calorim. 2021;143(2):1021–1035.

[39] Zeeshan A, Ijaz N, Bhatti MM, et al. Mathematical study of peristaltic propulsion of solid–liquid multiphase flow with a biorheological fluid as the base fluid in a duct. Chin J Phys. 2017;55(4):1596–1604.

[40] Riaz A, Nadeem S, Ellahi R. Effects of the wall properties on unsteady peristaltic flow of an Eyring–Powell fluid in a three-dimensional rectangular duct. Int J Biomath. 2015;08:1550081.